# Prototype electrostatic ground state approach to predicting crystal structures of ionic compounds: Application to hydrogen storage materials

E. H. Majzoub*
*Department of Physics and Astronomy, Center for Nanoscience, University of Missouri, St. Louis, Missouri 63121, USA*

V. Ozoliņš
*Department of Materials Science and Engineering, University of California, Los Angeles, California 90095-1595, USA*
(Received 5 September 2007; published 18 March 2008)

We have developed a procedure for crystal structure generation and prediction for ionic compounds consisting of a collection of cations and rigid complex anions. Our approach is based on global optimization of an energy functional consisting of the electrostatic and soft-sphere repulsive energies using Metropolis Monte Carlo (MMC) simulated annealing in conjunction with smoothing of the potential energy landscape via the distance scaling method. The resulting structures, or prototype electrostatic ground states (PEGS), are subsequently relaxed using first-principles density-functional theory (DFT) calculations to obtain accurate structural parameters and thermodynamic properties. This method is shown to produce the ground state structures of $NaAlH_4$ and $Mg(AlH_4)_2$, as well as the mixed cation alanate $K_2LiAlH_6$. For $LiAlH_4$, the PEGS search produces a structure with a static DFT total energy equal to that of the experimentally observed structure; the latter is stabilized by vibrational contributions to the free energy. For mixed-valence hexa-alanates, $XY$ $AlH_6$, where $X=(Li,Na,K)$, and $Y=(Mg,Ca)$, the PEGS method predicts six unsuspected structure types, which are not found in the existing structure databases. The PEGS search yields energies that are, on the average, better than the best database structures with the same number of atoms per unit cell, demonstrating the predictive power and usefulness of the PEGS structures. In addition to the recently synthesized $LiMgAlH_6$ compound, we predict that $LiCaAlH_6$, $NaCaAlH_6$, and $KCaAlH_6$ are also thermodynamically stable with respect to phase separation into other alanates and metal hydrides. In contrast, $NaMgAlH_6$ and $KMgAlH_6$ are slightly unstable (by less than 3 kJ/mol) relative to the phase separation into $NaAlH_4$, $KAlH_4$, and $MgH_2$. We suggest that solid-state ion-exchange reactions between $X_3AlH_6$ $(X=Li,Na,K)$ and $YCl_2$ $(Y=Mg,Ca)$ could be used to synthesize the predicted mixed-valence hexa-alanates.

DOI: 10.1103/PhysRevB.77.104115 PACS number(s): 78.30.Hv, 63.20.−e, 65.40.De, 77.22.−d

## I. INTRODUCTION

Finding a light-weight, high-density means for hydrogen storage is one of the key bottlenecks towards the large-scale introduction of hydrogen-fueled vehicles. Traditionally, interstitial metal hydrides have been considered for this purpose since they can store hydrogen at very high volumetric densities, easily surpassing liquid hydrogen. However, the gravimetric density of reversibly stored hydrogen in these systems is typically only a couple percent, which is unacceptably low for commercial applications.[1] Research on hydrogen storage materials took a new direction in 1997 with the discovery that sodium aluminum hydride, $NaAlH_4$, becomes a reversible solid-state hydrogen storage material upon the addition of a small amount (a few percent) of transition metal dopants.[2,3] This discovery more than doubled the gravimetric storage capacity of classic interstitial metal hydrides, from about 1.5–2.0 wt. % $H_2$ in compounds such as $LaNi_5$, to about 5 wt. % in sodium alanate. It also led to the realization that the whole class of compounds based on anionic complexes, such as $AlH_4^-$, $AlH_6^{-3}$, $BH_4^-$, and $NH_2^-$, charge balanced by a cation matrix, are potential high-density light-weight hydrogen storage candidates.

The complex ionic hydrides such as $NaAlH_4$, $LiAlH_4$, and corresponding borohydrides were initially synthesized and used as reducing agents in solution.[4] Unsolvated $NaAlH_4$ is a wide band gap insulator and can be viewed as a molecular ionic solid.[5,6] First-principles calculations of the electronic structure of many of the complex ionic hydrides indicate analogous behavior.[5,7–9] Upon decomposition, the complex ionic hydrides typically decompose to other stoichiometric compounds. For example, both sodium alanate, $NaAlH_4$, and lithium alanate, $LiAlH_4$, decompose through the reactions in Eqs. (1) and (2), releasing hydrogen and forming bulk aluminum as follows:

$$M\mathrm{AlH_4} \rightarrow \tfrac{1}{3}M_3\mathrm{AlH_6} + \tfrac{2}{3}\mathrm{Al} + \mathrm{H_2}, \quad (1)$$

$$M_3\mathrm{AlH_6} \rightarrow 3M\mathrm{H} + \mathrm{Al} + \tfrac{3}{2}\mathrm{H_2}, \quad (2)$$

where $M=$Li or Na. One of the key materials requirements for engineering applications is the enthalpy of hydrogen desorption, defined as the enthalpy change upon releasing one mole of $H_2$. The enthalpy provides an important link between the temperature range of use and the equilibrium pressure of the hydrogen gas. Classic interstitial hydrides in use today, as well as new materials such as sodium alanate, have endothermic desorption enthalpies in the range of 30–50 kJ/mol $H_2$. High decomposition enthalpies, such as 75 kJ/mol $H_2$ for $MgH_2 \rightarrow Mg+H_2$, tend to indicate that the material will have a hydrogen equilibrium pressure of around 1 bar at temperatures high compared to 100 °C, the range needed to utilize polymer electrolyte membrane fuel cell waste heat. Indeed, the equilibrium pressure of $MgH_2$ at 250 °C is only

 

about 0.4 bar.[10] Low decomposition enthalpies, such as in the case of $Ca(AlH_4)_2$,[11,12] correspond to materials that have equilibrium pressures of 500 bars at very low temperatures and therefore are not easily rehydrided under practical conditions. It is of significant interest to determine these enthalpies for materials where measurement is difficult or which have not yet been synthesized.

First-principles calculations within the density-functional theory (DFT) are a powerful tool for calculating the thermodynamic properties of known materials, and they have been used extensively for this purpose. A knowledge of the crystal structures is required for the calculation of the enthalpy of the decomposition reactions such as Eqs. (1) and (2),[5] but unfortunately this information is often unavailable. For instance, only a few mixed cation alanates, such as $K_2LiAlH_6$ (Ref. 13) and $LiMgAlH_6$,[14] have been synthesized and solved. Crystalline forms of Ca and Mg borohydrides have been synthesized only recently,[15–17] and almost nothing is known about the existence, stability, and structure of mixed cation borohydrides, such as $LiMg(BH_4)_3$. In cases where crystal structures are not available, and when the samples may not be easy to synthesize and characterize, the predictive power of first-principles methods is greatly diminished by the inability to determine the crystal structure theoretically. It can be argued that determination of the ground state crystal structures using first-principles energetics remains one of the key unsolved problems in computational materials science.

One method that has recently gained popularity is the so-called *database searching method,* which considers candidate crystal structures of chemically similar compounds from published databases, such as the Inorganic Crystal Structure Database (ICSD). This method amounts to choosing reasonable crystal structure types ("rounding up the usual suspects") and calculating their total energies with DFT techniques; it was first adopted in theoretical studies of high-pressure structural stability.[18] With the increase in the available computer power, larger and larger sets of trial structures have become practical. For instance, a recent study of $Ca(AlH_4)_2$ and $CaAlH_5$ used sets of 93 and 83 trial structures, respectively.[12] The data mining technique offers an efficient way to focus this search by selectively choosing the likeliest ground states.[19] However, these methods rely heavily on the existence of an extensive database of good trial structures and are incapable of generating new crystal structure types in the absence of information on similar compounds. The cluster expansion technique allows one to efficiently search the configuration space of alloys, but it is currently limited to lattice-based systems.[20] Recently, genetic algorithms have emerged as promising methods of finding new ground state crystal structures in systems that either have diffraction data or can be described by classical potentials,[21] but the computational expense of first-principles DFT calculations for large systems currently limits their applicability to unit cells with a few tens of atoms.[22,23] Methods based on first-principles variable cell shape molecular dynamics[24] can be used to accurately explore structural transformation paths, but they require the user to supply a "good" starting structure and are difficult to apply when such data are not available. Monte Carlo based techniques have been used for the structure determination of a wide range of systems, from finite clusters[25] and organic molecules,[26] to crystalline solids.[27–29] Due to their versatility and generality, these methods are capable of predicting not only the ground states, but also entropically stabilized phases.[25] However, with a few notable exceptions,[21] Monte Carlo methods have been seldom used systematically in conjunction with accurate first-principles DFT energetics in the search for new materials. Such applications usually require extensive and time-consuming fitting of interatomic potentials.[28] Nonergodic search methods have also been explored with some success toward solving the structure of Lennard-Jones clusters and small molecules,[30] but have not yet been tried for complex bulk crystals with multiple ionic species.

This paper will present a global optimization method for generating crystal structures and determining first-principles $T=0$ K total energies for complex ionic compounds, which does not rely on the existence of structural prototypes and does not require the development of accurate interatomic potentials. Our method allows for generation of new structure types based on classical considerations such as ionic charges and ionic radii, and is therefore applicable in cases when crystal structures of chemically similar compounds are not available. Accurate DFT forces and energetics are used to reliably find optimized structural parameters and thermodynamic properties. We find unsuspected crystal structures for compound stoichiometries that are not currently contained in structural databases, resulting in an important contribution to these databases. Section II will outline the method and provide justification of the physical model. Results for hydrogen storage materials will be given in Sec. III. Discussion of the results and implications for materials searching are given in Sec. IV.

## II. METHODS

### A. Prototype electrostatic ground state (PEGS) search

Complex ionic hydrides share several common features in the electronic structure and bonding, which constitute the physical basis for our approach. First, complex hydrides are typically wide gap insulators, with strongly bound $AlH_4^-$, $AlH_6^{3-}$, or $BH_4^-$ anionic complexes. Second, first-principles DFT calculations of a large number of hypothetical structures using the structure database searching approach (see Sec. II B) indicate that the anion complexes have very similar shapes and charge states in all low-energy crystal structures. Third, it has been pointed out by several researchers that the electrostatic interactions between the cations and anions play a key role in determining the stable crystal structure type.[5,9,36] Fourth, experimental structures taken from diffraction data of tetrahydride alanates indicate that the anion center to vertex lengths are within a few percent of each other. Finally, Raman studies of the lattice dynamics of both borohydrides and alanates indicate that internal anion vibrations are distinct and well separated from the crystal translational and librational modes.[6,31–35]

The above observations suggest that candidate ground states for complex hydrides may be found by minimizing the electrostatic energy of a collection of positively charged cat-

ions and negatively charged complex anions (e.g., $AlH_4$ tetrahedra and $AlH_6$ octahedra), with the latter treated as rigid units. This idea is analogous to the classical approach used in the classification of ionic crystal structure types based on the ionic charges and radii of the constituents. In the simplest case of binary ionic compounds, elementary geometric considerations can accurately predict the regions of stability of fourfold (zinc-blende), sixfold (rocksalt), and eightfold (CsCl, fluorite) coordinated binary crystal structures with increasing ratio of the cation-to-anion radii.[37] In this paper, we generalize this approach to complex hydrides by considering complexes instead of spherical anions. New ground state structure types are generated by minimizing the electrostatic energy of a system of spherical cations and geometrically complex anions, subject to constraints on interionic distances imposed by the ionic radii of the constituents. These ground states are identified as functions of the parameters describing the ionic radii and charge distribution in the system, and a map of structure types, called prototype electrostatic ground states (PEGS), can be constructed to cover the parametric region representing the system of interest. The resulting PEGS are used as input to first-principles DFT calculations to obtain accurate total energies and structural coordinates.

The energy functional used in our Monte Carlo approach is given in Eq. (3) below. For each complex anion, all center to hydrogen distances and all bond angles are kept fixed. Ionic repulsion at short distances is introduced via a soft sphere interaction potential with fixed values of ionic radii for all species in the system. There is one value for $\epsilon_{ss}=1$ in Eq. (3) for all ion pairs in the soft-sphere interaction, which is large enough to prevent any overlap at low temperatures:

$$E_{\mathrm{tot}} = \sum_{i>j} \frac{Q_i Q_j}{R_{ij}} + \sum_{i>j} \frac{\epsilon_{ss}}{R_{ij}^{12}}. \tag{3}$$

The first term is the Coulomb energy, with $Q_i$ denoting the ionic charges. The second term is a repulsive, soft-sphere potential, taken from the repulsive part of a Lennard-Jones 6-12 potential, which *only contributes when ion cores overlap*. Both sums extend over all ions in the system, including the center and vertex ions comprising the rigid complex anions but excluding ion pairs comprising the same complex. The radius of the anion center ion does not impact the resulting PEGS. The input parameters for the Metropolis Monte Carlo (MMC) runs include the radii of the cations, vertex anions, and their charges. Procedures for choosing these parameters are described below. Here we only note that the Hamiltonian Eq. (3) is *not* meant to accurately represent all the details of the interionic interactions in complex hydrides, just like the rigid ion model is not meant to represent the details of the interactions in systems like NaH. We are interested in identifying new prototype structures with exceptionally low electrostatic energies; the detailed structural parameters and energetics will be obtained using state-of-the-art DFT methods.

Given the energy functional in Eq. (3), the structure generation algorithm can be summarized as follows. First a simulated annealing of the lattice parameter and cell contents, consisting of a collection of rigid anions charge balanced by cations, is performed according to the Metropolis algorithm, with the total energy given by Eq. (3). Following the MMC minimization, the structure is fully relaxed via DFT.

There are four different configuration changes, which are effected in random order during the Metropolis run. Detailed balance is maintained at each step to ensure the *a priori* probability for the system to return to a previous configuration.

(i) Lattice parameter changes. The lattice vectors of the unit cell are defined by $\bar{a}_1, \bar{a}_2, \bar{a}_3$. The angles between the lattice vectors are defined by $\alpha \equiv \bar{a}_2 \angle \bar{a}_3$, $\beta \equiv \bar{a}_3 \angle \bar{a}_1$, and $\gamma \equiv \bar{a}_1 \angle \bar{a}_2$. Either a lattice vector is changed in magnitude, or one of the angles between lattice vectors is altered. The change in either lattice vector magnitude or direction is limited to a maximum volume change of the unit cell of 7%. The lattice angles are bounded by a lower limit of 10°, and an upper limit of 120°. Additional constraints are provided by a parameter *orth*, defined as the ratio of the cell volume to the volume of an orthogonal cell with identical lattice vector magnitudes. The *orth* parameter was bounded by 0.2 below, to prevent unit cell "squashing" to zero volume. The primitive cell of fcc NaCl has a value of $orth=0.7071$. Additionally, any two planes of the unit cell were limited to a distance no closer than 1.5 times the distance between the anion center and anion vertex.

(ii) Cation or anion translations. The maximum translation length along direction $\alpha=\bar{a}_1$, $\bar{a}_2$, or $\bar{a}_3$ was $\frac{|\alpha|}{2}$.

(iii) Anion rotations. The three Euler angles describing the orientation of a rigid body are chosen randomly and the anion is rotated according to the generated rotation matrix.

(iv) Swapping of anion and cation locations. Anions are swapped with cations such that the anion center is exchanged with the location of the cation. The anion is not rotated.

Using an exponential annealing schedule, the temperature is given by $T_{\mathrm{hi}} e^{[-n^3/T_\alpha]}$, where $n=1,\ldots,N$. The total number of temperature runs is $N$. The temperature $T_\alpha$ is calculated for given initial and final temperatures, $T_{\mathrm{hi}}$ and $T_{\mathrm{low}}$, respectively. The high and low temperatures for the anneal are taken from an autoadjusting algorithm described below.

From the partition function in the canonical ensemble, at constant particle number ($N$), volume ($V$), and temperature ($T$), one finds that the specific heat in terms of the energy fluctuations is given by

$$C_{\mathrm{NVT}} = \frac{\langle U^2 \rangle - \langle U \rangle^2}{k_B T^2}. \tag{4}$$

In our Metropolis algorithm we hold temperature and particle number constant, allowing the volume to vary, and calculate a pseudospecific heat using Eq. (4). Approximate temperature ranges corresponding to the liquid melt were determined by investigating plots of the mean square energy fluctuations versus temperature. We set the initial temperature at the onset of condensation, and the final temperature near the peak in the energy fluctuations. The mean square energy fluctuations for NaCl are shown in Fig. 1. The fluctuations (noise) in the figure are indicative of small energy fluctuations at low temperature, which occur when the num-

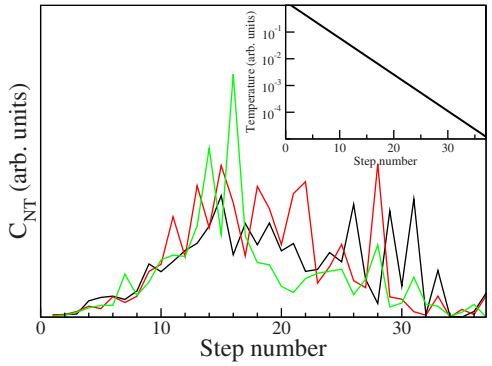


FIG. 1. (Color online) Three identical Monte Carlo simulated annealing minimizations showing the mean square energy fluctuations (the pseudoheat capacity $C_{NT}$) in one formula unit of NaCl. The inset shows the temperature in arbitrary units for each step.

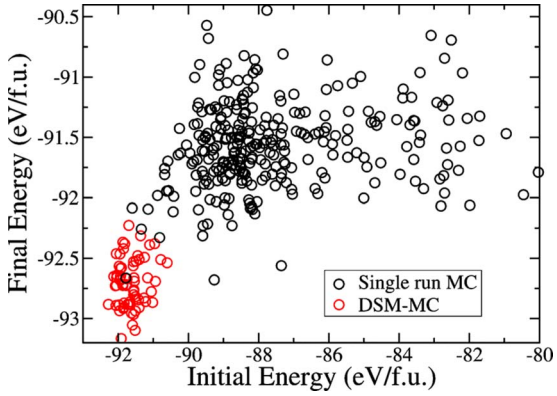


FIG. 2. (Color online) Initial and final (after relaxation) DFT energies for MC generated structures of two formula units of $Ca(BH_4)_2$. The black circles show multiple runs of MC only. The red/gray circles show distance scaling method DSM-MC. Initial DFT total energies are significantly lower using the DSM-MC method, indicating superior structure generation over single run MC.

ber of configuration changes is too small to reach equilibrium. This was not found to be problematic in generating low-energy crystal structures. The region of temperature is set using short, fixed-temperature anneals, and adjusted based on the percentage rejection rate of a choice of the four allowed configuration changes. The onset of condensation corresponds to lattice parameter and translation rejection rates in the range 67.5–72.5 %. The peak in energy fluctuations occurs for rejection rates of between 95% and 99.9%.

During the anneal, the electrostatic and repulsive energies are calculated for each structure after every configuration change. A record is kept of the lowest total energy structure, defined by the sum of the electrostatic and repulsive energies. Following the simulated anneal, the lowest energy structure is compared to the structure obtained at the end of the run. In the event that the total energy of the final structure is higher, and the difference between the electrostatic energies is greater than the difference of the respective repulsive energies, then the structures are swapped. Using the total energy alone is not sufficient to prevent a situation where a large repulsive energy difference dominates the total energy difference, and a structure with lower electrostatic energy is discarded. The structure swap is justified by the quick relaxation and elimination of the repulsive energy by the simplex routine which follows. Once the simulated anneal has been completed, the system is further relaxed using the downhill simplex method, and removes overlap completely at the end of the simulated anneal.

Two methods were employed to improve the energies obtained by standard MMC. First was the Monte Carlo with minimization (MCM) and coordinate resetting procedure of Li and Scheraga, known as basin hopping.[38] In this method one performs repeated resetting of the initial coordinates followed by the Metropolis algorithm and a minimization procedure such as simplex, or conjugate gradient. At the end of the minimization, and before resetting the coordinates, the structure is compared to the previously accepted local minimum. The second method employed was the distance scaling method (DSM) of potential energy smoothing (PES), hereafter referred to as DSM-MC.[39] A scaling of the atom-atom distances $r' = \alpha r$, reduces the repulsive energy for $\alpha > 1$, and allows atoms to overlap while the configuration changes rearrange the cations and anions subject to a reduced electrostatic interaction. The DSM-MC method results in dramatic improvement in the structures generated as illustrated in Fig. 2, which shows the initial and final (relaxed) DFT total energies of structures generated for the compound $Ca(BH_4)_2$ through the MMC and DSM-MC approach. Details of the DFT calculations for this compound are given in Sec. II C.

PEGS structures generated through MCM basin hopping, or DSM-MC are subsequently relaxed using VASP, yielding optimized cell volume, shape, and ionic positions. The structures are then searched for symmetry using the FINDSYM program in the ISOTROPY package using an rms displacement tolerance of around 0.1 Å.[40]

The above procedure is summarized in the following steps.

1. Atomic radii, anion bond lengths, and number of formula units per cell are chosen.
2. Initial and final annealing temperatures are taken from calculated rejection percentages.
3. The cell contents are initialized with random fractional coordinates. No previous information on cell parameters or similar structure types is used in the global optimization.
4. MCM basin hopping or DSM-MC generates an intermediate (PEGS) structure with minimum electrostatic energy. The cell parameters, including both lattice parameters and angles between the lattice vectors, are optimized along with the fractional coordinates of the anion centers, anion angles, and cation centers.
5. The PEGS structure is fully relaxed using first-principles DFT.
6. The final output structure is searched for symmetry.

Step 4 requires multiple steps, including coordinate resetting, in the case of MCM basin hopping, or reversing of the scaling parameter in the case of DSM-MC.

The anion coordination and bond lengths are taken from experimental diffraction data and/or first-principles calculations on known materials. For example, the Al–H bond lengths in four- and six-coordinated alanates are taken as

TABLE I. Aluminum-hydrogen bond lengths and charges used for ions comprising the rigid anionic $AlH_4^-$ and $AlH_6^{3-}$ units. Ion charges are taken from first-principles calculated Born effective charges.

| | Anion type | |
|---|---|---|
| | $AlH_4^-$ | $AlH_6^{3-}$ |
| $d_{Al\text{-}H}$ | 1.6500 | 1.7800 |
| $Q_{Al}$ | +1.6700 | +2.0000 |
| $Q_H$ | −0.6675 | −0.8333 |
| $R_H$ | 1.5000 | 1.3500 |

1.65 and 1.78 Å, respectively.[5] Ionic charges are obtained from first-principles calculated Born effective charges by averaging the diagonal elements for all symmetry-distinct ion types, as shown in Table I. Nominal ionic radii of the cations were taken from standard tables for ions in their inert gas configuration.[41] Radii for Li, Na, K, Mg, and Ca were taken as 0.68, 0.97, 1.33, 0.65, and 0.99 Å, respectively. Radii of the aluminum anion centers were taken from the difference of the center to vertex distance and the radii of the hydrogen atoms, $d$-$R_H$. Optimal hydrogen radii were determined by examination of the $M$-H minimum distances in initial DFT-relaxed PEGS structures, where $M$ is *not* the anion center atom, to determine new input values for $R_H = d_{M\text{-}H} - R_M$.

### B. Database searching

A commonly employed method of structure determination involves the use of a database such as the Inorganic Crystal Structure Database (ICSD), containing over 93 000 inorganic crystal structures.[42] In this approach, one searches the database for potential structures of chemically related compounds and calculates the DFT total energies for the compound of choice in those structures. The structure with lowest energy is presumed to be the ground state. The strength of any database-based searching method lies in the total number of potential structures available for a chosen stoichiometry or compound formula. For example, the compound $NaAlH_4$ would be searched for in the ICSD database using the "ANX formula" search string "*ABX*4," yielding over 1800 entries, and over 100 independent potential crystal structures. Database searching using the ICSD results in finding the correct structures for compounds $Be(BH_4)_2$, $Ca(AlH_4)_2$, and $Ca(BH_4)_2$, where the compound formula *AB*2*X*8 yields 270 entries and at least 50 unique structures. If the number of structures in which the (DFT) total energy is calculated is small, the probability of finding the correct structure is lower. The need for methods other than database searching is easily illustrated by the data in Table II showing the number of database entries for increasingly complicated compound stoichiometries.

### C. *Ab initio* energetics

Crystal binding energies were calculated using the first-principles total energy and molecular dynamics program Vienna *ab initio* simulation package (VASP).[43,44] Plane augmented wave (PAW) pseudopotentials[45,46] were used to represent the interactions between the ions and the valence electrons. Electron exchange-correlation interactions were treated in the generalized gradient approximation (GGA) using the Perdew-Burke-Ernzerhof (PBE) functional.[47] Electronic states were expanded in plane wave basis with an energy cutoff of 600 eV. The Brillouin zone for each structure was sampled with a Monkhorst-Pack mesh[48] using a $k$-point spacing of less than 0.05 $Å^{-1}$. All structures were relaxed using the conjugate gradient algorithm until the atomic forces were less than 0.01 eV/Å and the stresses were below 0.001 kbar. High-accuracy test calculations for $LiAlH_4$ structures were performed using PAW pseudopotentials and the Perdew-Wang[49] GGA exchange-correlation functional with a plane wave cutoff of 875 eV. Phonon frequencies were calculated using the supercell frozen phonon force constant method, using a plane wave energy cutoff of 600 eV. A detailed description of this implementation can be found elsewhere.[6]

In most cases (except $LiAlH_4$), we have ignored contributions to the total energy due to phonons, since the main purpose of this work is to develop and test a new method for crystal structure prediction using *static* DFT energetics. This level of accuracy is sufficient for determining whether a given material warrants further attention and calculation of the phonon contributions. We note here that vibrational contributions have been shown to lower the $T=0$ K decomposition enthalpies by as much as 20 kJ/mol $H_2$; the effect on room-temperature enthalpies is usually smaller, but can amount to a lowering of $\Delta H$ by as much as 10 kJ/mol $H_2$.[50]

TABLE II. Number of Inorganic Crystal Structure Database (ICSD) entries for common compound types.

| ICSD "*ANX*" formula | Example | Number of entries |
|---|---|---|
| *AB*2*X*8 | $Ca(BH_4)_2$ | 271 |
| *ABCX*6 | $LiCaAl_6$ | 158 |
| *AB*2*C*4*X*16 | $CaLi_2(BH_4)_4$ | 27 |
| *ABC*3*X*12 | $CaLi(BH_4)_3$ | 15 |

## III. RESULTS

Structural energy minimizations were performed for simple cases such as NaCl, CsCl, and $CaF_2$ to confirm that the code would produce the correct structures. Results for the more complicated structures of known alanates $NaAlH_4$, $LiAlH_4$, $Mg(AlH_4)_2$, and $K_2LiAlH_6$ will be presented here.

### A. Sodium alanate $NaAlH_4$

The experimentally determined crystal structure of $NaAlH_4$ is body centered tetragonal with space group number 88, $I4_1/a$.[51] The conventional tetragonal cell, containing four formula units, has first-principles optimized lattice vector lengths of $a=4.98$ Å, $c=11.06$ Å. The primitive cell volume is 137.06 $Å^3$. Parameters for the DSM-MC minimization were $Q_H=-0.6675$, $Q_{Al}=1.67$, $d_{Al\text{-}H}=1.65$ Å, $R_H$

TABLE III. Lattice vector and fractional atom position output for one DSM-MC global optimization of two formula units of $NaAlH_4$. DFT relaxation of this structure yields the experimentally observed crystal structure in space group $I4_1/a$. The ground state structure is found in approximately 20% of DSM-MC runs.

| DSM-MC PEGS output for $NaAlH_4$ | | | |
|---|---|---|---|
| | $x$ | $y$ | $z$ |
| $a$ | 6.50665944 | 0.00000000 | 0.00000000 |
| $b$ | −2.15168706 | 4.59090657 | 0.00000000 |
| $c$ | 2.30170864 | 4.05164112 | 4.53675796 |
| $Na_1$ | 0.98126288 | 0.83373802 | 0.54291502 |
| $Na_2$ | 0.73528823 | 0.32796480 | 0.29136268 |
| $Al_1$ | 0.24154350 | 0.35018111 | 0.78949297 |
| $Al_2$ | 0.49434981 | 0.84844347 | 0.02814165 |
| $H_1$ | 0.25941245 | 0.24194315 | 0.58046735 |
| $H_2$ | 0.10614212 | −0.02318605 | 1.10998862 |
| $H_3$ | 0.57646513 | 0.73676861 | 0.62479864 |
| $H_4$ | 0.02415431 | 0.44519874 | 0.84271726 |
| $H_5$ | 0.66831083 | 1.23549211 | −0.30795578 |
| $H_6$ | 0.44848149 | 0.95119652 | 0.24146781 |
| $H_7$ | 0.16808868 | 0.48254873 | 0.16150051 |
| $H_8$ | 0.69251825 | 0.72453650 | 0.01755405 |

$=1.3$ Å, and $R_{Na}=0.97$ Å. Calculated Born effective charges supplied the charge values used for Al and H.[6] The output atom positions of the DSM-MC structure are given in Table III as an example and proof of the method. In this and subsequent PEGS output results, we give enough significant figures for reproducibility. The $AlH_4$ tetrahedra in the DSM-MC PEGS output are undistorted, with all center to vertex lengths equal. A first-principles optimization (using PAW pseudopotentials and the PBE[47] exchange-correlation functional with 600 eV cutoff) of the lowest-energy two formula unit electrostatic structure shown in Table III yields an energy within 0.2 meV of the experimentally determined structure, with identical symmetry found using FINDSYM. Generally, about 20% of DSM-MC runs produce PEGS structures which yield equivalent ground state structures. Post-DFT relaxation of the $NaAlH_4$ PEGS structure, the magnitudes of the lattice vectors are $a=6.54$, $b=6.54$, and $c=4.99$ Å, with angles $\alpha=112.42°$, $\beta=67.68°$, and $\gamma=65.13°$, with a cell volume of 133.4 Å$^3$, indicating the primitive cell was located. *For this material, a DSM-MC search finds the ground state crystal structure*.

### B. Lithium alanate $LiAlH_4$

Lithium alanate, $LiAlH_4$, has crystal symmetry $P2_1/c$, with lattice parameters of the deuteride refined as $a=4.825$ Å, $b=7.804$ Å, $c=7.897$ Å, $\alpha=\gamma=90°$, and $\beta=112.268°$, with a cell volume of 53.46 Å$^3$ per formula unit.[52] The crystal retains this structure down to 8 K as indicated by diffraction data. Our calculated DFT relaxed lattice parameters for the $P2_1/c$ structure are in good agreement with the results of other DFT calculations,[53] and agree to within 2% with the experimental values. The radius of the Li cation used in the DSM-MC minimization was 0.68 Å. All other minimization parameters were identical to those used for $NaAlH_4$ above. Performing a DSM-MC minimization using a two formula unit cell results in a structure of $P\bar{1}$ symmetry. The lattice parameters of the DFT relaxed PEGS structure, using PAW pseudopotentials and the PBE exchange-correlation[47] (xc) functional, were $a=6.12$ Å, $b=5.07$ Å, and $c=5.14$ Å, with a cell volume of 75.49 Å$^3$ per formula unit. DFT calculations using both the ultrasoft and PAW pseudopotentials and the PBE xc functional indicate that the PEGS structure is 7 meV below the experimentally observed $P2_1/c$ structure, while calculations using the PAW potentials and Perdew-Wang GGA[49] functional place the PEGS structure 9 meV above the experimental structure. This suggests that *the static energies of the $P2_1/c$ and $P\bar{1}$ structures are degenerate within the error bars of the calculation determined by the accuracy of the pseudopotentials and xc functionals*.

TABLE IV. Phonon free energy contributions for $LiAlH_4$ supercells. Units are eV per formula unit.

| Supercell | | Zero-point | $T=300$ K |
|---|---|---|---|
| Experiment | $2\times1\times1$ | 0.812 | 0.708 |
| Experiment | $2\times2\times2$ | 0.807 | 0.710 |
| Experiment | 12 cell | 0.814 | 0.695 |
| PEGS | $1\times1\times1$ | 0.821 | 0.751 |
| PEGS | $2\times2\times2$ | 0.834 | 0.728 |

We further evaluated the effect of vibrational free energy on the relative structural stability of the $P2_1/c$ and $P\bar{1}$ structures. Lattice vibration frequencies were calculated using the supercell frozen phonon method discussed in Sec. II C. Phonon convergence calculations were performed for three supercells for the experimental $P2_1/c$ structure and two supercells for the PEGS structure. The lattice parameters for the PEGS structure are close to a distorted cubic, and supercells of $1\times1\times1$ (12 atoms), and $2\times2\times2$ (96 atoms) were used. Three experimental structure supercells were (i) $1\times1\times1$ (24 atoms), (ii) $2\times1\times1$ (48 atoms), and (iii) the supercell closest to a cubic (containing 12 unit cells), with lattice vectors given by $\vec{SC}_1=1\vec{a}+2\vec{c}$, $\vec{SC}_2=2\vec{b}$, $\vec{SC}_3=3\vec{c}$ (288 atoms) (Table IV). Results of our calculation of the total free energy including contributions from lattice vibrations are shown in Fig. 3. No soft modes (imaginary phonon frequencies) or other anomalies were observed in the calculated phonon spectra of either the experimentally observed $P2_1/c$ or the $P\bar{1}$ structure. We note that our total free energy calculations for the $P2_1/c$ structure, including phonon contributions in the harmonic approximation, are in good agreement with those of Ke and Chen.[53] Because the $P2_1/c$ and $P\bar{1}$ structures are essentially degenerate in their static energies, we show only the phonon free energies as a function of temperature in Fig. 3, without adding the $T=0$ K ($E_0$) energy. The ZPE of the $P\bar{1}$ structure is 20 meV above the $P2_1/c$ experi-

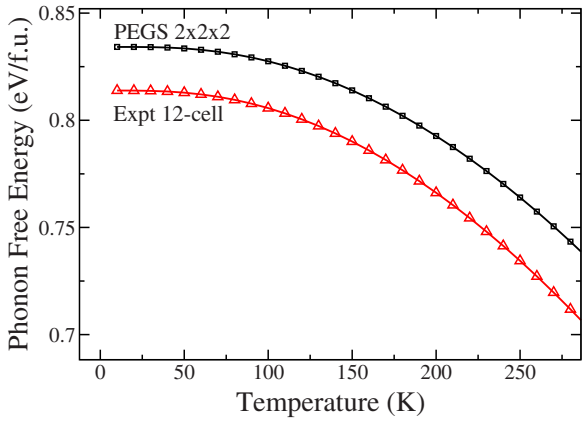


FIG. 3. (Color online) The phonon free energy $E_{vib}+TS_{vib}$ for supercell structures of $LiAlH_4$. The DFT-relaxed PEGS structure energy at $T=0$ K is within a few meV per formula unit of the experimentally observed structure. The vibrational contribution to the free energy lowers the experimentally observed structure below the PEGS structure for all temperatures.

mental structure at $T=0$ K, and the total free energy of the $P2_1/c$ structure is below that of $P\bar{1}$ for all temperatures. Therefore, we conclude that the $P2_1/c$ structure is stabilized by vibrational free energy. The importance of vibrational effects in determining the ground state structure of $LiAlH_4$ is consistent with the fact that this compound has the lowest average atomic mass among all compounds considered.

### C. Magnesium alanate $Mg(AlH_4)_2$

Magnesium alanate, $Mg(AlH_4)_2$, crystallizes in the hexagonal space group $P\bar{3}m1$ with lattice parameters $a=5.208$ Å and $c=5.839$ Å.[54] The primitive cell contains one formula unit. A one formula unit DSM-MC minimization was performed using a $Mg^{2+}$ cation radius of 0.65 Å, and identical $AlH_4^-$ parameters as described above for $NaAlH_4$. The results are shown in Table V. A first-principles optimization (PAW pseudopotentials and the PBE exchange-correlation functional, with 600 eV cutoff) of the lowest-energy electrostatic structure yields an energy within 0.1 meV of the experimentally determined structure, with identical symmetry found using FINDSYM. We again find the ground state crystal structure.

### D. Calcium alanate $Ca(AlH_4)_2$

Calcium alanate, $Ca(AlH_4)_2$, evidently takes the structure of the related fluoride $Ca(BF_4)_2$ in space group *Pbca*, determined by a thorough first-principles database search.[12] The *Pbca* fluoride structure contains eight formula units, or 88 atoms, in the primitive cell. Eight formula units is prohibitively large for a DSM-MC search to complete in a reasonable amount of time. DSM-MC searches using one and two formula units each were performed for comparison using a $Ca^{2+}$ ionic radius of 0.99 Å, and the anion parameters as given in Table I. A one formula unit search finds a structure in space group $R\bar{3}$, with an energy 25 kJ/mol above the fluoride structure. A two formula unit search finds a structure in space group $P4/nnc$, with an energy of only 8.4 kJ/mol above the fluoride structure. These results indicate that if the number of formula units in the primitive cell is insufficient to reproduce the global ground state, the PEGS search will obtain a total energy quickly approaching the ground state as the number of formula units used in the DSM-MC search increases.

TABLE V. Lattice vector and fractional atom position output for one DSM-MC global optimization of one formula unit of $MgAl_2H_8$. First-principles structural relaxation yields symmetry $P\bar{3}m1$, as well as identical energy to the experimentally observed structure.

| DSM-MC PEGS output for $MgAl_2H_8$ | | | |
|---|---|---|---|
| | *x* | *y* | *z* |
| *a* | 5.56922581 | 0.00000000 | 0.00000000 |
| *b* | 2.70265721 | 6.86667289 | 0.00000000 |
| *c* | 2.76148157 | −3.11921248 | 3.58598099 |
| $Mg_1$ | 0.00446601 | 0.39810276 | 0.17068643 |
| $Al_1$ | 0.37071655 | 0.70758247 | 0.14022670 |
| $Al_2$ | 0.63819438 | 0.08964744 | 0.20125463 |
| $H_1$ | 0.62491939 | 0.61344310 | 0.21540100 |
| $H_2$ | 0.64275255 | 0.58720272 | −0.29531591 |
| $H_3$ | 0.14575583 | 0.60404287 | 0.21551647 |
| $H_4$ | 0.06943845 | 1.02564118 | 0.42530523 |
| $H_5$ | 0.93778647 | −0.22822469 | −0.07994651 |
| $H_6$ | 0.38007032 | 0.18214762 | 0.12961728 |
| $H_7$ | 0.36971531 | 0.21328932 | 0.63828217 |
| $H_8$ | 0.86520544 | 0.19137752 | 0.11706558 |

### E. Potassium-lithium alanate $K_2LiAlH_6$

The bialkali alanate $K_2LiAlH_6$ crystallizes in space group $R\bar{3}m$, with lattice parameters $a=5.621$ Å and $c=27.399$ Å, respectively.[13] The $\frac{c}{a}$ ratio is large, and the crystal structure contains six formula units per conventional hexagonal cell, which can be defined in a trigonal primitive cell with two formula units. An ICSD database search of this compound yields the observed crystal structure.[13] The two database structures $K_2LiAlF_6$ ($R\bar{3}m$) and $Cs_2NaAlF_6$ ($C2/m$) have energies within a few kJ/mol per formula unit. All other database structures have energies 10 kJ/mol f.u. or higher above the ground state. A DSM-MC search was performed with two formula units using $Li^+$ and $K^+$ radii of 0.68 and 1.33 Å, respectively. Anion parameters are given in Table I. The atomic coordinates of the PEGS structure are shown in Table VI. First-principles structural relaxation yields symmetry $R\bar{3}m$, as well as identical energy to the experimentally observed structure, showing that the PEGS search is able to reproduce the observed ground state of $K_2LiAlH_6$.

The results obtained when the ionic parameters are not chosen optimally (e.g., when charges are not those defined by the Born effective charge) are also found to be useful. As

TABLE VI. Lattice vector and fractional atom position output for one DSM-MC global optimization of two formula units of $K_2LiAlH_6$. DFT relaxation of this structure results in $R\bar{3}m$ symmetry, the observed structure.

| DSM-MC PEGS output for $K_2LiAlH_6$ | | | |
|---|---|---|---|
| | $x$ | $y$ | $z$ |
| $a$ | 5.74472981 | 0.00000000 | 0.00000000 |
| $b$ | 1.72669580 | 9.51981331 | 0.00000000 |
| $c$ | 2.76971900 | −0.50031622 | 4.80453959 |
| $K_1$ | 0.65929854 | 0.00017342 | 0.27499563 |
| $K_2$ | 0.43717713 | 0.75434912 | 0.89137915 |
| $K_3$ | 0.81102843 | 0.27331060 | 0.66265735 |
| $K_4$ | 0.42187604 | 0.48076587 | 0.37015586 |
| $Li_1$ | 0.77747179 | 0.68130539 | 0.21688599 |
| $Li_2$ | 0.20636859 | 0.11682813 | 0.00427869 |
| $Al_1$ | 0.04804748 | 0.88275441 | 0.57818349 |
| $Al_2$ | 0.11629168 | 0.37792000 | 0.01517882 |
| $H_1$ | −0.27135800 | 1.00437065 | 0.71667259 |
| $H_2$ | 0.36745296 | 0.76113817 | 0.43969439 |
| $H_3$ | 0.19323202 | 0.98083010 | 0.28644716 |
| $H_4$ | −0.09713706 | 0.78467872 | 0.86991983 |
| $H_5$ | −0.05243773 | 0.77820440 | 0.39661175 |
| $H_6$ | 0.14853270 | 0.98730443 | 0.75975523 |
| $H_7$ | 0.27574497 | 0.27679102 | 0.18090785 |
| $H_8$ | −0.04316160 | 0.47904897 | −0.15055021 |
| $H_9$ | −0.09619779 | 0.49463085 | 0.32601244 |
| $H_{10}$ | 0.32878115 | 0.26120915 | −0.29565481 |
| $H_{11}$ | −0.13394533 | 0.27072128 | 0.12995670 |
| $H_{12}$ | 0.36652870 | 0.48511871 | −0.09959907 |

an example, we give the PEGS structure for a DSM-MC search for $K_2LiAlH_6$ using suboptimal hydrogen ion charges $Q_H=-0.5$. The other parameters for the DSM-MC minimization are as follows: $Q_{Al}=0$, $d_{Al\text{-}H}=1.78$ Å, $R_H=1.35$ Å, $R_K=1.33$ Å, and $R_{Li}=0.68$ Å. A two formula unit PEGS structure, after DFT relaxation, yields a crystal with lattice parameters $a=5.62$ Å and $c=9.17$ Å (about 1/3 of the experimental $c$-axis length) in the space group $P6_3mc$. This structure, with atomic coordinates given in Table VII, was not found in the ICSD database. The energy of the $P6_3mc$ structure is only 1.2 kJ/mol f.u. above the ground state $R\bar{3}m$ structure, demonstrating that even a suboptimal choice of parameters can produce practically useful estimates of the hydrogenation enthalpies. In fact, the error inherent in the DFT is thought to be much larger than the $P6_3mc/R\bar{3}m$ energy difference, on the order of 10 kJ/mol $H_2$.[55] Thus, the PEGS method here again demonstrates its usefulness in suggesting unsuspected crystal structure prototypes.

The similarity of the local order in the experimentally observed crystal and the DFT-relaxed PEGS structure is shown in the total pair distribution function in Fig. 4. In the case of suboptimal choice of parameters, the DSM-MC method predicts a small-unit-cell PEGS structure, which can be used to obtain a very accurate estimate of the enthalpy, more than sufficient to evaluate the stability and practical usefulness of the material for hydrogen storage.

TABLE VII. An unsuspected structure type for ICSD "*ANX*" formula $A_2BCX_6$ discovered in a PEGS search for $K_2LiAlH_6$.

| Atom | Wyckoff site | $x$ | $y$ | $z$ |
|---|---|---|---|---|
| | $P6_3mc$ $a=b=5.61634$, $c=9.17422$ $\alpha=\beta=90$, $\gamma=120$ | | | |
| K | 2*b* | 1/3 | 2/3 | 0.26862 |
| K | 2*a* | 0 | 0 | 0.01538 |
| Li | 2*b* | 1/3 | 2/3 | 0.91092 |
| Al | 2*b* | 2/3 | 1/3 | 0.13711 |
| H | 6*c* | 0.96928 | 0.48464 | 0.02722 |
| H | 6*c* | 0.37947 | 0.18973 | 0.25597 |

### F. Mixed valence hexa-alanates

We have performed PEGS searches for the following $AlH_6$-based compounds: $LiMgAlH_6$, $NaMgAlH_6$, $KMgAlH_6$, $LiCaAlH_6$, $NaCaAlH_6$, and $KCaAlH_6$. Out of these, only $LiMgAlH_6$ has been reported previously;[14] our results for the five other compounds are pure predictions. Using DSM-MC runs with one and two formula unit cells, we have obtained eight new high-symmetry structure types with low electrostatic energies. These structures are shown in Table VIII, which gives their symmetries, cell parameters, Wyckoff positions, and the systems that they were derived from [defining the ionic radii used in the PEGS Hamiltonian Eq. (3)]. These structures are unsuspected and currently not found in an ICSD search for *ABCX*6 structure types. The structures are therefore valuable as additions to the database literature. In addition to those listed in Table VIII, the PEGS search also found structures that already exist in the ICSD,

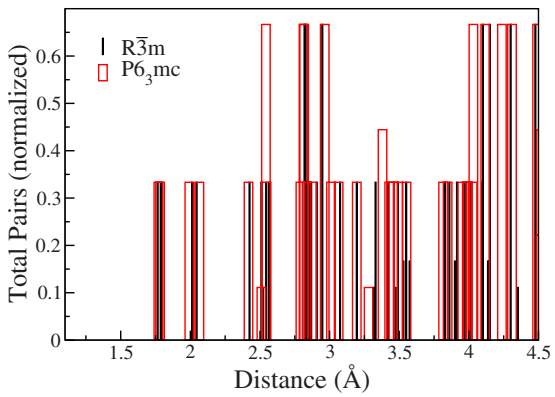


FIG. 4. (Color online) Total pair distribution functions for $K_2LiAlH_6$. The experimental structure with symmetry $R\bar{3}m$ (black bars) and the DSM-MC structure with symmetry $P6_3mc$ (red/gray bars), are similar in local order out to more than 4.5 Å. The distribution function for the DSM-MC structure was calculated after DFT relaxation and a search for the symmetry with the program FINDSYM (Ref. 40).

TABLE VIII. New structure types for $ABCX_6$ compounds not found in the ICSD database. Note that these structures are not necessarily the lowest-energy structures discovered through the PEGS search (see Table IX).

| Atom | Wyckoff site | $x$ | $y$ | $z$ | Atom | Wyckoff site | $x$ | $y$ | $z$ |
|---|---|---|---|---|---|---|---|---|---|
| | | | | $LiMgAlH_6$ | | | | | |
| | $Fdd2$ $a$=5.64978, $b$=7.23269, $c$=17.82076 | | | | | $C2/c$ $a$=8.42123, $b$=7.98019, $c$=5.72490 | | | |
| | $\alpha=\beta=\gamma=90$ | | | | | $\alpha=90$, $\beta=85.68044$, $\gamma=90$ | | | |
| Li | 8*a* | 1/4 | 1/4 | 0.40794 | Li | 4*e* | 0 | 0.55010 | 3/4 |
| Mg | 8*a* | 1/2 | 1/2 | 0.51337 | Mg | 4*e* | 0 | 0.06721 | 1/4 |
| Al | 8*a* | 1/4 | 1/4 | 0.25019 | Al | 4*c* | 3/4 | 1/4 | 1/2 |
| H | 16*b* | 0.51470 | 0.25239 | 0.68688 | H | 8*f* | 0.15257 | 0.75968 | 0.78197 |
| H | 16*b* | 0.46355 | 0.24225 | 0.32208 | H | 8*f* | 0.60793 | 0.40610 | 0.42585 |
| H | 16*b* | 0.73024 | 0.50963 | 0.24536 | H | 8*f* | 0.12093 | 0.59467 | 0.44140 |
| | | | | $NaMgAlH_6$ | | | | | |
| | $R3$ $a=b$=4.96851, $c$=25.12207 | | | | | $I\bar{4}$ $a=b$=5.12617, $c$=7.38163 | | | |
| | $\alpha=\beta=90$, $\gamma=120$ | | | | | $\alpha=\beta=\gamma=90$ | | | |
| Na | 6*a* | 0 | 0 | 0.15221 | Na | 2*d* | 1/2 | 0 | 1/4 |
| Na | 6*a* | 0 | 0 | 0.72676 | Mg | 2*a* | 0 | 0 | 0 |
| Mg | 6*a* | 0 | 0 | 0.86968 | Al | 2*b* | 0 | 0 | 1/2 |
| Mg | 6*a* | 0 | 0 | 0.01288 | H | 4*e* | 0 | 0 | 0.73731 |
| Al | 6*a* | 0 | 0 | 0.27680 | H | 8*g* | 0.27042 | 0.20482 | 0.49701 |
| Al | 6*a* | 0 | 0 | 0.44278 | | | | | |
| H | 18*b* | 0.69696 | 0.70461 | 0.31603 | | | | | |
| H | 18*b* | 0.96068 | 0.59817 | 0.56821 | | | | | |
| H | 18*b* | 0.89761 | 0.66721 | 0.40406 | | | | | |
| H | 18*b* | 0.10594 | 0.32948 | 0.48133 | | | | | |
| | | | | $KMgAlH_6$ | | | | | |
| | $R3$ $a=b$=4.92446, $c$=35.44539 | | | | | $Amm2$ $a$=5.79989, $b$=5.60071, $c$=7.27616 | | | |
| | $\alpha=\beta=90$, $\gamma=120$ | | | | | $\alpha=\beta=\gamma=90$ | | | |
| K | 6*a* | 0 | 0 | 0.56392 | K | 2*a* | 0 | 0 | 0.48371 |
| K | 6*a* | 0 | 0 | 0.72574 | Mg | 2*b* | 1/2 | 0 | 0.21650 |
| Mg | 6*a* | 0 | 0 | 0.14012 | Al | 2*b* | 1/2 | 0 | 0.73207 |
| Mg | 6*a* | 0 | 0 | 0.97678 | H | 8*f* | 0.71261 | 0.77036 | 0.72767 |
| Al | 6*a* | 0 | 0 | 0.30971 | H | 2*b* | 1/2 | 0 | 0.96263 |
| Al | 6*a* | 0 | 0 | 0.47068 | H | 2*b* | 1/2 | 0 | 0.49036 |
| H | 18*b* | 0.96813 | 0.27461 | 0.28086 | | | | | |
| H | 18*b* | 0.97729 | 0.69582 | 0.33800 | | | | | |
| H | 18*b* | 0.98182 | 0.70066 | 0.50031 | | | | | |
| H | 18*b* | 0.96512 | 0.27462 | 0.44274 | | | | | |
| | | $KCaAlH_6$ | | | | | $NaCaAlH_6$ | | |
| | $Pmn2_1$ $a$=5.20257, $b$=9.38224, $c$=4.19822 | | | | | $R3$ $a=b$=5.28835, $c$=14.39207 | | | |
| | $\alpha=\beta=\gamma=90$ | | | | | $\alpha=\beta=90$, $\gamma=120$ | | | |
| K | 2*a* | 1/2 | 0.92000 | 0.57215 | Na | 6*a* | 0 | 0 | 0.52037 |
| Ca | 2*a* | 1/2 | 0.58238 | 0.05940 | Ca | 6*a* | 0 | 0 | 0.73674 |
| Al | 2*a* | 1/2 | 0.26857 | 0.80762 | Al | 6*a* | 0 | 0 | 0.23447 |
| H | 2*a* | 1/2 | 0.43107 | 0.57895 | H | 18*b* | 0.90049 | 0.63919 | 0.63388 |
| H | 2*a* | 1/2 | 0.11727 | 0.03338 | H | 18*b* | 0.42749 | 0.04230 | 0.49354 |
| H | 4*b* | 0.73961 | 0.36338 | 0.03463 | | | | | |
| H | 4*b* | 0.24667 | 0.20815 | 0.57814 | | | | | |

TABLE IX. Comparison of $T=0$ K DFT $E_0$ energies (in kJ/mol) for the low-energy structures from the database and PEGS searches. Energies are given relative to the lowest-energy structure found in this study.

| f.u. | ICSD-prototype | Energy | f.u. | PEGS-prototype | Energy |
|---|---|---|---|---|---|
| | | $LiCaAlH_6$ | | | |
| 4 | $LiBaCoF_6$ ($P2_1/c$) | 0.0 | 2 | $LiMgAlH_6$ ($Fdd2$) | 8.5 |
| 4 | $NaSrFeF_6$ ($P2_12_12_1$) | 1.2 | 2 | $LiCaAlH_6$ ($P1$) | 11.0 |
| 4 | $NaKSnF_6$ ($Pna2_1$) | 4.0 | | | |
| 4 | $NaSrCrF_6$ ($P2_1/c$) | 5.4 | | | |
| 2 | $LiSmAlF_6$ ($P6_322$) | 12.1 | | | |
| | | $NaCaAlH_6$ | | | |
| 4 | $KNaSiF_6$ ($Pnma$) | 0.0 | 2 | $KCaAlH_6$ ($R3$) | 13.1 |
| 3 | $LiMnGaF_6$ ($P321$) | 12.3 | 2 | $KCaAlH_6$ ($Pmn2_1$) | 14.8 |
| 4 | $NaSrFeF_6$ ($P2_12_12_1$) | 13.4 | 2 | $LiMgAlH_6$ ($P2_12_12$) | 15.0 |
| 8 | $NaSrAlF_6$ ($oP72$) | 13.6 | 2 | $LiCaAlH_6$ ($P1$) | 15.6 |
| 4 | $LiSrAlF_6$ ($P2_1/c$) | 14.6 | 2 | $LiMgAlH_6$ ($C2/c$) | 15.6 |
| 8 | $NaCaAlF_6$ ($P2_1/c$) | 15.2 | 1 | $NaCaAlH_6$ ($P1$) | 19.4 |
| 4 | $KNaSiF_6$ ($Pnma$) | 15.8 | | | |
| 4 | $LiSrCoF_6$ ($P2_1/c$) | 15.8 | | | |
| 4 | $NaKSnF_6$-2 ($Pna2_1$) | 19.2 | | | |
| 4 | $NaSrCrF_6$ ($P2_1/c$) | 20.4 | | | |
| 4 | $NaKSnF_6$ ($Pna2_1$) | 22.6 | | | |
| 4 | $KCuGaF_6$ ($P2_1/c$) | 25.1 | | | |
| 8 | $NaRbSnF_6$ ($Pbcn$) | 28.7 | | | |
| 2 | $CoTeMoO_6$ ($P2_12_12$) | 29.5 | | | |
| | | $KCaAlH_6$ | | | |
| 4 | $KNaSiF_6$-2 ($Pnma$) | 0.0 | 2 | $LiMgAlH_6$ ($P2_12_12_1$) | 22.2 |
| 8 | $NaCaAlF_6$ ($P2_1/c$) | 22.3 | 2 | $KCaAlH_6$ ($Pmn2_1$) | 22.3 |
| 8 | $NaSrAlF_6$ ($oP72$) | 35.7 | 2 | $KCaAlH_6$ ($R3$) | 23.0 |
| 4 | $NaSrCrF_6$ ($P2_1/c$) | 35.8 | | | |
| 4 | $NaSrFeF_6$ ($P2_12_12_1$) | 36.1 | | | |
| 3 | $LiMnGaF_6$ ($P321$) | 39.0 | | | |
| 4 | $CsNiNiF_6$ ($Imma$) | 39.7 | | | |
| 2 | $RbMgAlF_6$ ($Fd3$-$MZ$) | 39.7 | | | |
| | | $LiMgAlH_6$ | | | |
| 3 | $LiMnGaF_6$ ($P321$) | 0.0 | 2 | $LiCaAlH_6$ ($P1$) | 6.7 |
| 4 | $NaSrFeF_6$ ($P2_12_12_1$) | 2.0 | 2 | $LiMgAlH_6$ ($P2_12_12$) | 6.8 |
| 2 | $LiCaAlF_6$ ($P\bar{3}1C$) | 5.8 | | | |
| | | $NaMgAlH_6$ | | | |
| 2 | $BaGeTeO_6$ ($P312$) | 0.0 | 1 | $NaMgAlH_6$ ($P312$) | 0.0 |
| 1 | $RbGeIO_6$ ($P312$) | 0.1 | 1 | $NaCaAlH_6$ ($P1$) | 0.0 |
| 2 | $RbSnIO_6$ ($P6_322$) | 1.8 | 2 | $KMgAlH_6$ ($P6_322$) | 2.1 |
| | | | 2 | $KMgAlH_6$ ($R3$) | 7.0 |
| | | $KMgAlH_6$ | | | |
| 4 | $CsAgAlF_6$ ($Pnma$) | 0.0 | 2 | $KMgAlH_6$ ($P6_322$) | 9.6 |
| 4 | $KCuCrF_6$ ($P2_1/c$) | 0.0 | 1 | $NaCaAlH_6$ ($P1$) | 9.8 |
| 2 | $RbMgAlF_6$ ($Fd3$-$MZ$) | 3.9 | 1 | $NaMgAlH_6$ ($P312$) | 9.8 |
| | | | 2 | $KMgAlH_6$ ($R3$) | 17.1 |
| | | | 1 | $KMgAlH_6$ ($Amm2$) | 21.3 |

TABLE X. Comparison of the energetics for the best small-unit-cell structures found from ICSD and PEGS searches. "ICSD 2 f.u." and "PEGS 2 f.u." give the energy difference in kJ/mol of structures with two or fewer formula units relative to the ground state.

| System | Ground state | ICSD 2 f.u. | PEGS 2 f.u. |
|---|---|---|---|
| $LiMgAlH_6$ | 3 f.u.-$LiMnGaF_6$ ($P321$) | +5.8 | +6.7 |
| $NaMgAlH_6$ | 1 f.u.-$RbGeIO_6$ ($P312$) | 0 | 0 |
| $KMgAlH_6$ | 4 f.u.-$CsAgAlF_6$ ($Pnma$) | +3.9 | +9.6 |
| $LiCaAlH_6$ | 4 f.u.-$LiBaCoF_6$ ($P2_1/c$) | +12.1 | +8.5 |
| $NaCaAlH_6$ | 4 f.u.-$KNaSiF_6$ ($Pnma$) | +29.5 | +13.1 |
| $KCaAlH_6$ | 4 f.u.-$KNaSiF_6$ ($Pnma$) | +39.7 | +22.2 |

such as the $P2_12_12_1$ and $P6_322$ structures, which were derived for $LiMgAlH_6$ and $KMgAlH_6$, respectively. Interestingly, we have found low electrostatic energy structures with $P1$ symmetries for $LiCaAlH_6$ and $NaCaAlH_6$; this might be a manifestation of geometric frustration in trying to accommodate size-mismatched cations in unit cells that are limited to only two formula units. The coordinates of these $P1$ structures are not given in Table VIII, since they are not expected to be observed in nature. For each compound, we have calculated the fully relaxed DFT total energies of all the low-energy PEGS structures from Table VIII. This procedure increases the robustness of the PEGS search by allowing variations in the ionic radii of the cations, which are known only approximately for each compound, and may vary with both the chemical composition and coordination.

To establish the predictive abilities of the PEGS search, we have conducted an extensive database searching based on known $ABCX6$ compounds from the ICSD. Our trial set consisted of the following 28 structures (symmetry and prototype): $P312$ $RbGeIO_6$, $Fd\bar{3}m$ $RbMgAlF_6$, $P\bar{3}$ $KNaThF_6$, $P2_1/m$ $KHoBeF_6$, $P312$ $BaGeTeO_6$, $P6_322$ $RbSnIO_6$, $P2_12_12$ $CoTeMoO_6$, $P\bar{3}1c$ $LiCaAlF_6$, $P4_2nm$ $LiFe2F_6$, $P6_322$ $LiSmAlF_6$, $P321$ $LiMnGaF_6$, $P321$ $MnNaCrF_6$, $Cmcm$ $BaTe2O_6$, $Pnma$ $CsAgFeF_6$, $Pnma$ $KNaSiF_6$, $Pna2_1$ $NaKSnF_6$, $P2_1/c$ $LiSrAlF_6$, $P2_1/c$ $LiSrCoF_6$, $Pnma$ $RbAlPdF_6$, $P2_12_12_1$ $NaSrFeF_6$, $Imma$ $CsCuF_6$, $P2_1/c$ $NaSrCrF_6$, $P2_1/c$ $KCuCrF_6$, $Pna2_1$ $NaKSnF_6$, $P2_1/c$ $NaCaAlF_6$, $Pbcn$ $NaRbSnF_6$, $Pbcn$ $NaCsSnF_6$, and $Pna2_1$ $NaSrAlF_6$. For several of these structures ($NaCsSnF_6$, $NaKSnF_6$, $CoTeMo_6$, $KNaSiF_6$, and $KNaThF_6$) the assignment of alkali and alkaline earth cations to the lattice sites is not clear *a priori*, and we considered both of the possible assignments, giving a grand total of 33 trial structures. Initial DFT relaxations of atomic positions and unit-cell vectors were performed using ultrasoft pseudopotentials, followed by more accurate calculations on the 5–10 lowest-energy structures using the PAW method and the Perdew-Wang GGA.[49] We found that both methods produced very similar (usually, within 1–2 kJ/mol) total energy differences between the competing alanate phases at the same stoichiometry.

A comprehensive comparison of the energetics of the PEGS structures with the results of the ICSD search is given in Table IX. It shows that the ICSD search predicts ground states with three or more formula units for every system except $NaMgAlH_6$; in the latter case the PEGS and ICSD searches both find the same lowest-energy structure of $P312$ symmetry with one formula unit per cell. For the other compounds, the ICSD search predicts structures that are lower in energy than the PEGS structures, which we attribute to the limitations on the unit cell size that were imposed in our PEGS runs. A higher number of formula units would produce structures with lower energies, but would also require very long and expensive PEGS runs, which we have not undertaken here. These results show that large unit cells are needed to predict the ground states in many cases, further pointing to the importance of developing computationally efficient methods for suggesting new low-energy trial structures. To judge the relative performance of the PEGS and ICSD searches, we consider the ICSD predictions obtained from unit cells of *two or fewer formula units* in Table X. This table shows that PEGS outperforms ICSD for $LiCaAlH_6$, $NaCaAlH_6$, and $KCaAlH_6$, while for $LiMgAlH_6$ and $KMgAlH_6$ the predicted two formula unit ICSD structures are slightly lower in energy than the PEGS structures. We hypothesize that further tuning of the Mg ionic radius might increase the success of the PEGS search for the latter two compounds. Overall, the PEGS search outperforms ICSD searching if both are confined to structures with two formula units or less.

The calculated thermodynamic stabilities for all compounds in the lowest-energy structures are given in Table XI. The decomposition pathway was determined by minimizing the energy of the system with respect to all possible combi-

TABLE XI. Structural stabilities $\Delta H$ of the lowest-energy hexa-alanate structures identified in this study. The enthalpies are given relative to the energetically most favored phase separation products at each composition. Positive enthalpies indicate stable hexa-alanate compounds.

| Compound | Prototype (symmetry) | Products | $\Delta H$ (kJ/mol) |
|---|---|---|---|
| $LiMgAlH_6$ | $LiMnGaF_6$ ($P321$) | $\frac{1}{3}Li_3AlH_6+\frac{2}{3}MgAlH_5+\frac{1}{3}MgH_2$ | +16.5 |
| $NaMgAlH_6$ | $RbGeIO_6$ ($P312$) | $NaAlH_4+MgH_2$ | −2.5 |
| $KMgAlH_6$ | $CsAgAlF_6$ ($Pnma$) | $KAlH_4+MgH_2$ | −2.1 |
| $LiCaAlH_6$ | $LiBaCoF_6$ ($P2_1/c$) | $LiH+CaAlH_5$ | +4.1 |
| $NaCaAlH_6$ | $KNaSiF_6$ ($Pnma$) | $\frac{1}{3}Na_3AlH_6+\frac{2}{3}CaAlH_5+\frac{1}{3}CaH_2$ | +9.0 |
| | | $NaAlH_4+CaH_2$ | +9.1 |
| $KCaAlH_6$ | $KNaSiF_6$ ($Pnma$) | $KAlH_4+CaH_2$ | +8.5 |

TABLE XII. Predicted hydrogen release reactions and hydrogenation enthalpies for the mixed-cation hexa-alanates identified in this study. The calculated enthalpies are obtained from the static $T=0$ K DFT total energies and do not include vibrational contributions and the enthalpy of $H_2$ gas. The last column gives the gravimetric density of stored hydrogen relative to the starting mixed hexa-alanate.

| Reaction | $\Delta H_0$ (kJ/mol $H_2$) | Capacity (wt. % $H_2$) |
|---|---|---|
| $LiMgAlH_6 \rightarrow MgH_2 + \frac{2}{3}Al + \frac{1}{3}Li_3AlH_6 + H_2$ | +23.3 | 3.1 |
| $NaMgAlH_6 \rightarrow NaMgH_3 + Al + \frac{3}{2}H_2$ | +28.0 | 3.7 |
| $KMgAlH_6 \rightarrow KMgH_3 + Al + \frac{3}{2}H_2$ | +36.0 | 3.1 |
| $LiCaAlH_6 \rightarrow CaH_2 + LiH + Al + \frac{3}{2}H_2$ | +33.5 | 3.7 |
| $NaCaAlH_6 \rightarrow CaH_2 + \frac{2}{3}Al + \frac{1}{3}Na_3AlH_6 + H_2$ | +39.8 | 2.1 |
| $KCaAlH_6 \rightarrow CaH_2 + \frac{2}{3}Al + \frac{1}{3}K_3AlH_6 + H_2$ | +63.0 | 1.8 |

nations of binary and ternary hydrides using the linear programming approach developed in Ref. 50. The results indicate that all compounds, except $NaMgAlH_6$ and $KMgAlH_6$, are predicted to be stable with respect to phase separation into other alanates and hydrides. A thermodynamically feasible synthesis route might use ion-exchange reactions based on alkali hexa-alanates ball milled in a mixture with the corresponding alkaline earth chlorides as follows:

$$X_3AlH_6 + YCl_2 \rightarrow XYAlH_6 + 2XCl, \quad (5)$$

where $X$=Li,Na,K and $Y$=Mg,Ca. Our first-principles DFT calculations show that the energetics of this reaction are favorable for all six compounds from Table XI. This reaction may also be used in attempts to obtain the two compounds ($NaMgAlH_6$ and $KMgAlH_6$) that are predicted to be unstable, since the decomposition enthalpies are relatively small, suggesting that these compounds might be at least metastable. We have calculated the phonons for the lowest-energy $P312$ structure of $NaMgAlH_6$ using a $2\times2\times2$ supercell. We find that all the phonons are stable, indicating that this is indeed a physically reasonable one formula unit structure. Vibrational free energy contributions favor the phase separation of $NaMgAlH_6$ into sodium alanate and magnesium hydride by additional 5 kJ/mol at room temperature, mainly due to the higher vibrational entropy of sodium alanate. Furthermore, we see that most of the decomposition pathways in Table XI are quite nonintuitive, pointing to the importance of using nonbiased methods for evaluating thermodynamic stabilities, such as Ref. 50. For instance, in the case of $NaCaAlH_6$ there are two competing pathways, one of which involves the formation of $Na_3AlH_6$ and $CaAlH_5$, while the other involves $NaAlH_4$ and $CaH_2$.

The calculated hydrogenation enthalpies at $T=0$ K (without the zero-point vibrational energy contributions) are given in Table XII. Again, the thermodynamically favored decomposition pathway was obtained from the static DFT total energies of all known alkali and alkaline earth hydrides and alanates using the linear programming method of Ref. 50. These data show that all compounds release hydrogen endothermically, and that several of them ($NaMgAl_6$, $KMgAl_6$, $LiCaAl_6$, and $NaCaAl_6$) have hydrogenation enthalpies in the 25–40 kJ/mol $H_2$ range desired for reversible storage systems. Two general trends emerge from the data in Table XII. First, the hydrogen binding enthalpies tend to increase as one goes to heavier alkali metals (from Li to K), paralleling the trend observed in alkali tetra-alanates $X$ $AlH_4$. Second, the hydrogenation enthalpies of Ca compounds are substantially more endothermic than those of the Mg compounds. Including vibrational contributions and the enthalpy of the $H_2$ gas is expected to further lower these enthalpies by 5–10 kJ/mol $H_2$.[50,56] Even though the calculated theoretical gravimetric densities are below the long-term targets set for on-board hydrogen storage systems, some of the predicted reactions (especially $LiCaAlH_6$) appear interesting and experimental testing of our predictions is called for.

## IV. CONCLUSIONS

We have shown that the rigid anion electrostatics is a good approximation for determining the types and symmetries of the ground states in complex hydride alanates. Using Monte Carlo simulated annealing with the distance scaling method potential energy smoothing, we have been able to reproduce the ground state crystal structures for complicated complex hydrides including $NaAlH_4$, $MgAl_2H_8$, and $K_2LiAlH_6$. The PEGS method has identified several new unsuspected structures for compounds of the $ABCX6$ structure type as defined in the ICSD.[42] These structures will make useful additions to the database of high symmetry, low-energy structures for future searches. We also predict the existence of several new stable mixed-cation hexa-alanates ($LiCaAlH_6$, $NaCaAlH_6$, $KCaAlH_6$), and point to the possible metastability for the slightly unstable $NaMgAlH_6$ and $KMgAlH_6$ compounds. Finally, and most importantly, our results convincingly demonstrate that the symmetry and topology of ground state crystal structures of alanates, as well as those of most other complex hydrides (which will be considered in a future publication), can be understood in terms of simple electrostatics. This is a profound physical result which substantially enhances our understanding of the interatomic bonding and structure selection in this important class of materials, and may carry over to other complex ionic solids as well. The main advantage of our approach is that it obviates the need for an extremely time-consuming process of interatomic potential development for each new system

under study. A mature version of the PEGS code will be made available under the GNU public license (GPL).[57]

## ACKNOWLEDGMENTS

This work was funded by the U.S. Department of Energy, Office of Energy Efficiency and Renewable Energy, in the Hydrogen, Fuel Cells & Infrastructure Technologies Program under Contract No. DE-AC04-94AL85000. V.O. acknowledges financial support from the U.S. Department of Energy, Office of Sciences, Basic Energy Sciences under Contracts No. DE-FG02-05ER46253 and No. DE-FG02-07ER46433, and from the National Science Foundation Grant No. CBET-0730044.

*majzoube@umsl.edu

[1] G. Sandrock, J. Alloys Compd. **293-295**, 877 (1999).
[2] B. Bogdanovic and M. Schwickardi, J. Alloys Compd. **253**, 1 (1997).
[3] E. H. Majzoub and K. J. Gross, J. Alloys Compd. **356**, 363 (2003).
[4] A. E. Finholt, G. D. Barbaras, G. K. Barbaras, G. Urry, G. Wartik, and H. I. Schlesinger, J. Inorg. Nucl. Chem. **1**, 317 (1955).
[5] V. Ozolins, E. H. Majzoub, and T. J. Udovic, J. Alloys Compd. **375**, 1 (2004).
[6] E. H. Majzoub, K. F. McCarty, and V. Ozolins, Phys. Rev. B **71**, 024118 (2005).
[7] K. Miwa, N. Ohba, S. Towata, Y. Nakamori, and S. Orimo, Phys. Rev. B **69**, 245120 (2004).
[8] D. J. Siegel, C. Wolverton, and V. Ozoliņš, Phys. Rev. B **75**, 014101 (2007).
[9] B. Magyari-Köpe, V. Ozoliņš, and C. Wolverton, Phys. Rev. B **73**, 220101(R) (2006).
[10] Sandia National Laboratories, Hydride information database, http://hydpark.ca.sandia.gov
[11] M. Felderhoff, A. Pommerin, W. Schmidt, F. Schuth, M. Mamatha, B. Bogdanovic, and C. Weidenthaler, J. Alloys Compd. **407**, 78 (2006).
[12] C. Wolverton and V. Ozolins, Phys. Rev. B **75**, 064101 (2007).
[13] E. Ronnebro and E. H. Majzoub, J. Phys. Chem. B **110**, 25686 (2006).
[14] H. Grove, H. W. Brinks, O. M. Lovvik, R. H. Heyn, and B. C. Hauback, J. Alloys Compd. (to be published).
[15] J.-H. Her, P. W. Stephen, Y. Gao, G. C. Soloveichick, J. Rijssenbeek, M. Andrus, J.-C. Zhao, Acta Crystallogr. **B63**, 561 (2007.
[16] K. Miwa, M. Aoki, T. Noritake, N. Ohba, Y. Nakamori, S. Towata, A. Züttel, and S. Orimo, Phys. Rev. B **74**, 155122 (2006).
[17] E. Ronnebro and E. H. Majzoub, J. Phys. Chem. B **111**, 12045 (2007).
[18] A. Mujica and R. J. Needs, Phys. Rev. B **55**, 9659 (1997).
[19] S. Curtarolo, D. Morgan, K. Persson, J. Rodgers, and G. Ceder, Phys. Rev. Lett. **91**, 135503 (2003).
[20] V. Blum and A. Zunger, Phys. Rev. B **72**, 020104(R) (2005).
[21] T. S. Bush, C. R. A. Catlow, and P. D. Battle, J. Mater. Chem. **5**, 1269 (1995).
[22] A. R. Oganov and C. W. Glass, J. Chem. Phys. **124**, 244704 (2006).
[23] S. M. Woodley, Struct. Bonding (Berlin) **110**, 95 (2004).
[24] R. Martonak, A. Laio, and M. Parrinello, Phys. Rev. Lett. **90**, 075503 (2003).
[25] D. J. Wales and J. P. K. Doye, J. Phys. Chem. A **101**, 5111 (1997).
[26] Z. Li and H. A. Scheraga, Proc. Natl. Acad. Sci. U.S.A. **84**, 6611 (1987).
[27] J. Pannetier, J. Bassasalsina, J. Rodriguez-Carvajal, and V. Caignaert, Nature (London) **346**, 343 (1990).
[28] J. C. Schon and M. Jansen, Angew. Chem. **35**, 1287 (1996).
[29] A. Le Bail, J. Appl. Crystallogr. **38**, 389 (2005).
[30] S. Godecker, J. Chem. Phys. **120**, 9911 (2004).
[31] H. Hagemann, S. Gomes, G. Renaudin, and K. Yvon, J. Alloys Compd. **363**, 126 (2004).
[32] G. Renaudin, S. Gomes, H. Hagemann, L. Keller, and K. Yvon, J. Alloys Compd. **375**, 98 (2004).
[33] B. Bonnetot, P. Claudy, M. Diot, and J. M. Letoffe, J. Chem. Thermodyn. **11**, 1197 (1979).
[34] B. Bonnetot, G. Chahine, P. Claudy, M. Diot, and J. M. Letoffe, J. Chem. Thermodyn. **12**, 249 (1980).
[35] J.-C. Bureau, J.-P. Bastide, B. Bonnetot, and H. Eddaoudi, Mater. Res. Bull. **20**, 93 (1985).
[36] Y. Nakamori, K. Miwa, A. Ninomiya, H. Li, N. Ohba, S. Towata, A. Züttel, and S. Orimo, Phys. Rev. B **74**, 045126 (2006).
[37] W. D. Callister, *Materials Science and Engineering*, 7th ed. (John Wiley & Sons Inc., New York, 2007).
[38] Z. Q. Li and H. A. Scheraga, Proc. Natl. Acad. Sci. U.S.A. **84**, 6611 (1987).
[39] R. J. Wawak, J. Pillardy, A. Liwo, K. D. Gibson, and H. A. Scheraga, J. Phys. Chem. A **102**, 2904 (1998).
[40] H. T. Stokes and D. M. Hatch, Isotropy, http://stokes.byu.edu/isotropy.html, June 2006.
[41] C. Kittel, *Introduction to Solid State Physics*, 8th ed. (John Wiley and Sons, Inc., New York, 2005).
[42] Inorganic crystal structure database, http://icsd.ill.fr/icsd/index.html
[43] G. Kresse and J. Hafner, Phys. Rev. B **47**, 558 (1993).
[44] G. Kresse and J. Furthmüller, Comput. Mater. Sci. **6**, 15 (1996).
[45] P. E. Blöchl, Phys. Rev. B **50**, 17953 (1994).
[46] G. Kresse and D. Joubert, Phys. Rev. B **59**, 1758 (1999).
[47] J. P. Perdew, K. Burke, and M. Ernzerhof, Phys. Rev. Lett. **77**, 3865 (1996).
[48] H. J. Monkhorst and J. D. Pack, Phys. Rev. B **13**, 5188 (1976).
[49] J. P. Perdew and Y. Wang, Phys. Rev. B **45**, 13244 (1992).
[50] A. Akbarzadeh, V. Ozolins, and C. Wolverton, Adv. Mater. (Weinheim, Ger.) **19**, 3233 (2007).
[51] V. K. Bel'skii, B. M. Bulychev, and A. V. Golubeva, Russ. J. Inorg. Chem. **28**, 1528 (1983).
[52] B. C. Hauback, H. W. Brinks, and H. Fjellvag, J. Alloys Compd. **346**, 184 (2002).
[53] X. Ke and C. F. Chen, Phys. Rev. B **76**, 024112 (2007).
[54] A. Fossdal, H. W. Brinks, M. Fichtner, and B. C. Hauback, J. Alloys Compd. **387**, 47 (2005).
[55] C. Wolverton, V. Ozoliņš, and M. Asta, Phys. Rev. B **69**, 144109 (2004).
[56] D. J. Siegel, C. Wolverton, and V. Ozoliņš, Phys. Rev. B **76**, 134102 (2007).
[57] Information on the GNU Public License (GPL) can be obtained from the GNU website, http://www.gnu.org/copyleft/gpl.html